

Just Go with the Flow: Self-Supervised Scene Flow Estimation

Himangi Mittal
Carnegie Mellon University
hmittal@andrew.cmu.edu

Brian Okorn
Carnegie Mellon University
bokorn@andrew.cmu.edu

David Held
Carnegie Mellon University
dheld@andrew.cmu.edu

Abstract

When interacting with highly dynamic environments, scene flow allows autonomous systems to reason about the non-rigid motion of multiple independent objects. This is of particular interest in the field of autonomous driving, in which many cars, people, bicycles, and other objects need to be accurately tracked. Current state of the art methods require annotated scene flow data from autonomous driving scenes to train scene flow networks with supervised learning. As an alternative, we present a method of training scene flow that uses two self-supervised losses, based on nearest neighbors and cycle consistency. These self-supervised losses allow us to train our method on large unlabeled autonomous driving datasets; the resulting method matches current state-of-the-art supervised performance using no real world annotations and exceeds state-of-the-art performance when combining our self-supervised approach with supervised learning on a smaller labeled dataset.

1. Introduction

For an autonomous vehicle, understanding the dynamics of the surrounding environment is critical to ensure safe planning and navigation. It is essential for a self-driving vehicle to be able to perceive the actions of various entities around it, such as other vehicles, pedestrians, and bicyclists. In the context of 3D point clouds, this action is called scene flow. Scene flow refers to the 3D translation of each point in the scene providing us the velocity vector associated with every single point. It is the fundamental building block of motion for all semantic scene objects. Its 2D analog, optical flow, is the projection of scene flow onto the image plane of a camera. Previous methods use optical flow and the 3D structure of the environment [9] to estimate it, however, these methods do not make use of the depth information in estimation of the flow. Recent methods directly estimate the scene flow from 3D point clouds [10, 6, 24]. An alternative to scene flow estimation is to use 3D object detection for object-level tracking. But, in such a pipeline,

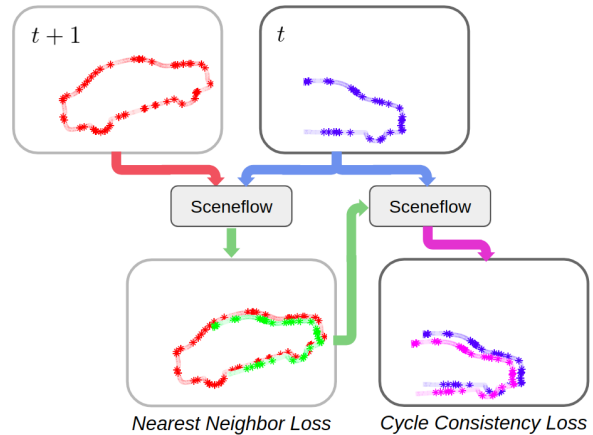


Figure 1: We use two self-supervised losses to learn scene flow on large unlabeled datasets. The “nearest neighbor loss” penalizes the distance between the predicted point cloud (green) and each predicted point’s nearest neighbor in the second point cloud (red). To avoid degenerate solutions, we estimate the flow between these predicted points (green) in the reverse direction back to the original point cloud (blue) to form a cycle. The new predicted points from the cycle (purple) should align with the original points (blue) and the distance between these two set of points, forms our second self-supervised loss: “cycle consistency.”

errors in object detection can lead to errors in tracking. In contrast, scene flow methods can avoid such errors by directly estimating the motion of each 3D point in the scene.

Recently, several methods have applied deep learning for scene flow estimation [10, 6]. These networks learn a hierarchical feature representation over point clouds to predict the flow for every point. However, these methods are fully supervised and require annotated datasets for training which are costly to obtain as they require labeling the motion for every point in a scene. To compensate for the lack of real world data, learning-based methods for scene flow have been trained primarily on synthetic datasets and fine tuned on real world data. This requirement of labeled training data limits the effectiveness of such methods in real world

settings.

To overcome this limitation, we propose a self-supervised method for scene flow estimation. Using a combination of two self-supervised losses, we are able to mimic the supervision created by human annotation. Specifically, we use a cycle consistency loss, which ensures that the scene flow produced is consistent in time (i.e. we ensure that temporal cycles end where they started). The flow is further regularized using a nearest neighbor loss. Due to the unavailability of scene flow annotation, we consider the nearest point to the predicted translated point in the temporally next point cloud as the pseudo-ground truth. The nearest neighbor loss operates by minimizing the euclidean distance between the predicted point and this pseudo-ground truth and impose further regularization to improve performance of our self-supervised approach. Intuitively, the nearest neighbor allows for the structure of one point cloud to flow toward occupied regions of the next point cloud. This combination of losses can be used to train scene flow methods over large-scale unannotated datasets containing sequential point cloud data. An overview of our method can be found in Figure 1.

We test our self-supervised training approach using the neural network architecture of the state-of-the-art scene flow method, FlowNet3D [10]. The self-supervision allows us to train on large-scale unlabeled autonomous driving datasets. Our method matches the current state-of-the-art performance when no real world annotations are given. Moreover, our method exceeds the performance of the state-of-the-art scene flow estimation methods when combined with supervised learning on a smaller labeled dataset.

The key contributions of our paper are as follows,

- We introduce a novel self-supervised training method for scene flow estimation using temporal cycle consistency, approximation of the correspondences with nearest neighbor, and dataset augmentation.
- We show that our self-supervised method can be applied to unannotated autonomous driving datasets to perform at-par with current state-of-the-art supervised approaches.
- We further show that our method is able to outperform state-of-the-art performance when combined with supervised learning on a smaller labeled dataset.

2. Related Work

Scene Flow Vedula *et al.* [20] first introduced it as a dense 3D vector field defined at every point in an environment. They propose a linear algorithm to compute it from optical flow. Other works involve joint optimization of camera extrinsics and depth estimates for stereo scene flow [18], use of particle filters [7], local rigid motion

priors [21, 23, 22, 12], and smoothness-based regularization [1].

Deep Scene Flow Liu *et al.* [10] presented the first method, called FlowNet3D, which used deep learning for scene flow estimation by learning directly on point clouds. This algorithm was trained entirely with labeled data. The supervised training consists of synthetically annotated data with a small amount of hand annotated real data used for fine tuning. FlowNet3D primarily comprises of three modules - point feature learning, point mixture, and flow refinement and three layers - set conv layer, flow embedding layer, and set upconv layer. It begins with hierarchically learning the point cloud features using its set conv layer inspired PointNet++ [17, 16], in the first module. In the next module, the flow embedding layer takes as input two point clouds of consecutive time steps, t and $t + 1$, and learns the flow vector for each point in the first point cloud. Following this, in the module of flow refinement, the set-upconv layer up-samples the learned flow embeddings by propagating the point features of the downsampled points (source points) to the actual points (target points). Lastly, a linear regression layer is used to output the scene flow. FlowNet3D shows substantial improvement after fine tuning their method on the annotated real world data, showing benefits of using real data along with the synthetic dataset. Gu *et al.* [6] produced similar results using a permutohedral lattice to encode the point cloud data in a sparse, structured manner and train it with supervised learning.

The above approaches use scene flow computed directly from 3D point clouds [10, 6]. Methods involving voxelizations with object-centric rigid body assumptions [2], range images [19], and non-grid structured data [24] have also been used in this field. Our approach is largely agnostic of the model used for scene flow estimation, since our method only relates to the loss used for training.

Self-Supervised Learning Wang *et al.* [26] used self-supervised learning for 2D tracking on video. They propose a tracker which takes a patch of an image at time t and the entire image at time $t - 1$ to track the image patch in the previous frame. They define a self-supervised loss by tracking the patch forward and backward in time to form a cycle while penalizing the errors through cycle consistency and feature similarity. We take inspiration from this work for our self-supervised flow estimation on point clouds. Other works including self-supervisory signals are image frame ordering [15], feature similarity over time [25] for images, and clustering and reconstruction [8] from point clouds. While these can potentially be used for representation learning from 3D data, they cannot be directly used for scene flow estimation.

3. Method

3.1. Problem Definition

For the task of scene flow estimation, we have a temporal sequence of point clouds: point cloud \mathcal{X} as the point cloud captured at time t and point cloud \mathcal{Y} captured at time $t + 1$. There is no structure enforced on these point clouds and they can be recorded directly from LIDAR sensor or estimated through a stereo algorithm. Each point $p_i = \{x_i, f_i\}$ in point cloud \mathcal{X} contains the Cartesian position of the point, $x_i \in \mathbb{R}^3$, as well as the additional information which the sensor produces, such as color, intensity, normals, etc, represented by $f_i \in \mathbb{R}^c$.

The scene flow, $\mathcal{D} = \{d_i\}^N, d_i \in \mathbb{R}^3$ between these two point clouds describes the movement of each Cartesian point x_i in point cloud \mathcal{X} to its corresponding position x'_i in the scene described by point cloud \mathcal{Y} , such that $x'_i = x_i + d_i$, where N is the size of point cloud \mathcal{X} . Scene flow is defined in a way such that x_i and x'_i represent the same 3D point of an object, moved in time. Unlike optical flow estimation, the exact 3D position of x'_i may not necessarily lie in the point cloud \mathcal{Y} . Additionally, the size of \mathcal{X} and \mathcal{Y} may be different.

Supervised Loss The true error associated with our task is the difference between the estimated flow $g(\mathcal{X}, \mathcal{Y}) = \hat{\mathcal{D}} = \{\hat{d}_i\}^N$ and the ground truth flow $\mathcal{D}^* = \{d_i^*\}^N$,

$$\mathcal{L}_{gt} = \frac{1}{N} \sum_i^N \|d_i^* - \hat{d}_i\|^2. \quad (1)$$

The loss in Equation 1 is useful because it is mathematically equivalent to the end point error, which will be described in the later sections as our evaluation metric. However, computing this loss requires annotated ground truth flow d_i^* . This type of annotation is easy to calculate in synthetic data [11], but requires expensive human labeling for real world datasets. As such, only a small amount of annotated scene flow datasets are available [13, 14]. While training on a purely synthetic data is possible, Lui *et al.* [10] showed an 18% relative improvement after fine-tuning on a small amount of annotated real world data. This result motivates our method of self-supervised training, allowing us to train on large unlabeled datasets.

Nearest Neighbor (NN) Loss For large unlabeled datasets, since we do not have information about d_i^* , we cannot compute the loss in Equation 1. In lieu of annotated data, we take inspiration from methods such as Iterative Closest Point [3] and use the nearest neighbor of our transformed point $\hat{x}'_i = x_i + \hat{d}_i$ as an approximation for the true correspondence. For each transformed point $\hat{x}'_i \in \hat{\mathcal{X}}'$,

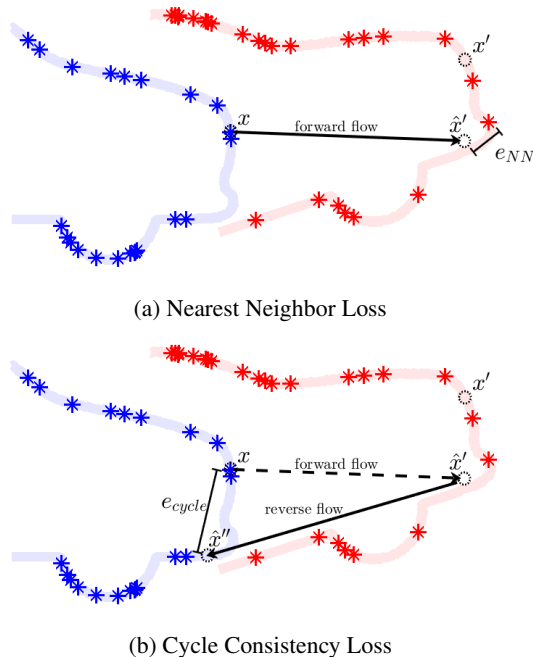


Figure 2: Example of our self-supervised errors between point clouds at time t , \mathcal{X} (blue), and $t + 1$, \mathcal{Y} (red). We consider the point x whose ground truth projected point x' is not known during training time. (a) Nearest Neighbor Loss is computed between the the projected point \hat{x}' , predicted by the forward flow, and the closest point in \mathcal{Y} . (b) The Cycle Consistency Loss tracks this transformed point back into its original frame, as point \hat{x}'' , using the reverse flow, and computes the distance to the original position x .

we find its nearest neighbor $y_j \in \mathcal{Y}$ and compute the Euclidean distance with that point, illustrated as e_{NN} in Figure 2a:

$$\mathcal{L}_{NN} = \frac{1}{N} \sum_i^N \min_{y_j \in \mathcal{Y}} \|\hat{x}'_i - y_j\|^2. \quad (2)$$

Assuming that the initial flow estimate is sufficiently close to the correct flow estimate, this loss will bring the transformed point cloud and the target point cloud closer. This loss can, however, have a few drawbacks if imposed alone. First, the true position of $x'_i = x_i + d_i^*$ may not be the same as the nearest neighbor to \hat{x}'_i , as illustrated in Figure 2a, due to potentially large errors in the estimated flow. Further, the position of x'_i may not correspond with any point in \mathcal{Y} if the point cloud \mathcal{Y} is sufficiently sparse, as is common for point clouds collected by sparse 3D LIDAR for autonomous driving. Finally, this loss does not penalize degenerate solutions where all of the points in \mathcal{X} map to the same point in \mathcal{Y} which might lead to the collapse of the entire predicted point cloud to only a handful of points

in point cloud \mathcal{Y} . To address these issues, we use an additional self-supervised loss, cycle consistency loss.

Cycle Consistency Loss To avoid these degeneracies, we incorporate an additional self-supervised loss: cycle consistency loss, illustrated in Figure 2b. We first estimate the “forward” flow as $\hat{D} = g(\mathcal{X}, \mathcal{Y})$. Applying the estimated flow $\hat{d}_i \in \hat{D}$ to each point $x_i \in \mathcal{X}$ gives an estimate of the location of the point x_i in the next frame: $\hat{x}'_i = x_i + \hat{d}_i$. We then compute the scene flow in the reverse direction: for each transformed point \hat{x}'_i we estimate the flow to transform the point back to the original frame, $\hat{D}' = g(\hat{\mathcal{X}}', \mathcal{X})$. Transforming each point \hat{x}'_i by this new “reverse” flow \hat{d}'_i gives a new estimated point \hat{x}''_i . If both the forward and reverse flow are accurate, this point \hat{x}''_i should be the same as the original point x_i . The error between these points, e_{cycle} , is the “cycle consistency loss,” given by

$$\mathcal{L}_{cycle} = \sum_i^N \|\hat{x}''_i - x_i\|^2. \quad (3)$$

A similar loss is used as regularization in [10].

Implementing the cycle loss in this way can produce unstable results, as errors in the estimated flow lead to structural distortions in $\hat{\mathcal{X}}'$. In order to maintain correspondences around the cycle, the transformed cloud $\hat{\mathcal{X}}'$ is used as an input in the reverse cycle $g(\hat{\mathcal{X}}', \mathcal{X})$. This requires the network to simultaneously learn to correct any distortions in $\hat{\mathcal{X}}'$, while also learning to estimate the true reverse flow. To solve this problem, we use the nearest neighbor y'_j of the transformed point \hat{x}'_i as an anchoring point in the reverse pass. Using the nearest neighbor y'_j stabilizes the structure of the transformed cloud while still maintaining the correspondence around the cycle. The effects of this stabilization are illustrated in Figure 3. As we are using the anchoring point as part of the reverse pass of our cycle, we refer to our cycle consistency loss as “anchored cycle consistency loss”.

We compute the anchored reverse flow, $\bar{D}' = \{\bar{d}'_i\}^N = g(\bar{\mathcal{X}}', \mathcal{X})$, with respect to the original point cloud \mathcal{X} , and the average of transformed point and its nearest neighbor $\bar{\mathcal{X}}' = \{\bar{x}'_i\}^N = \frac{1}{2}(\hat{x}'_i + y'_j)$. The local minima of each of the nearest neighbor and cycle losses conflict, allowing their sum, $\mathcal{L} = \mathcal{L}_{NN} + \mathcal{L}_{cycle}$, to act as a stable surrogate for the true error.

Temporal Flip Augmentation Having a dataset of point cloud sequences in only one direction may generate a motion bias which may lead to the network predicting the flow equal to the average forward speed of the training set. To reduce this bias, we augment the training set by flipping the point clouds, i.e, reversing the flow. With this augmentation, the network sees an equal number of point cloud se-

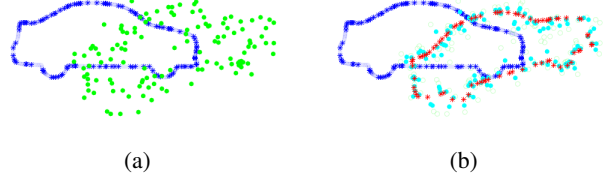


Figure 3: Compounding errors cause problems in estimating reverse flow using the transformed point cloud. (a) Large flow prediction errors degrade the structure of the transformed cloud $\hat{\mathcal{X}}'$ (shown in green). Thus, computing the reverse flow between $\hat{\mathcal{X}}'$ (green) and \mathcal{X} (blue) is an ill-posed task. (b) Using the anchor points of the nearest neighbor (red), we are able to stabilize the transformed cloud $\hat{\mathcal{X}}'$ (cyan), thus retaining important structural information.

quences having a forward motion as well as a backward motion.

4. Experiments

We run several experiments to validate our self-supervised method for scene flow estimation for various levels of supervision and different amounts of data. First, we compare the results of our self-supervised approach with the supervised fine tuning method [10]. Next, we investigate how our self-supervised method can generalize to the real world unannotated data by exploring both pure self-supervision as well as augmented supervised training. Finally, we explore the utility of each element of our method through an ablation study.

4.1. Implementation Details

For all data configurations (our method and the baseline), we initialize our network with the parameters of Flownet3D model pre-trained on FlyingThing3D dataset [11]. We compare our self-supervised training procedure to a fully supervised baseline which uses supervised fine-tuning on the KITTI dataset [5]. The method of the baseline used in the comparison is the same [10], however, we increase the training iterations from 150 epochs described in the original paper to 10k epochs in order to keep the training iterations consistent with the one used in our self-supervised method. We see that this change leads to a small improvement in the baseline performance, which we include in the results table.

4.2. Datasets

KITTI Vision Benchmark Suite KITTI [5] is a real-world self-driving dataset. There are 150 scenes of lidar data in KITTI collected using a Velodyne 64 lidar and annotated with ground truth scene flow. For our experiments under both self-supervised and supervised settings, we consider 100 out of 150 scenes for training and the remaining

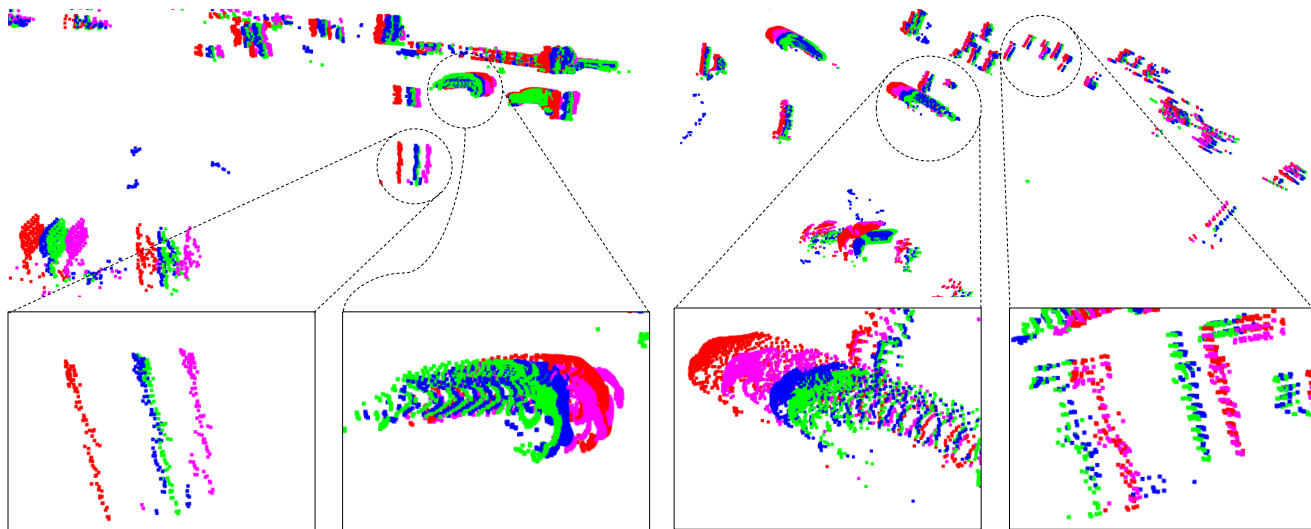


Figure 4: Scene flow estimation between point cloud at time t (red) and $t + 1$ (green) from KITTI dataset trained without any labeled lidar data. Our self-supervised method, trained on nuScenes and fine tuned on KITTI using self-supervised loss shown in blue and baseline training method, with no fine tuning, is shown in purple. All models are pretrained on FlyingThings3D using a supervised loss. In the absence of any lidar annotations, our method clearly outperforms the baseline method, which over estimate the flow in many regions. (Best viewed in color)

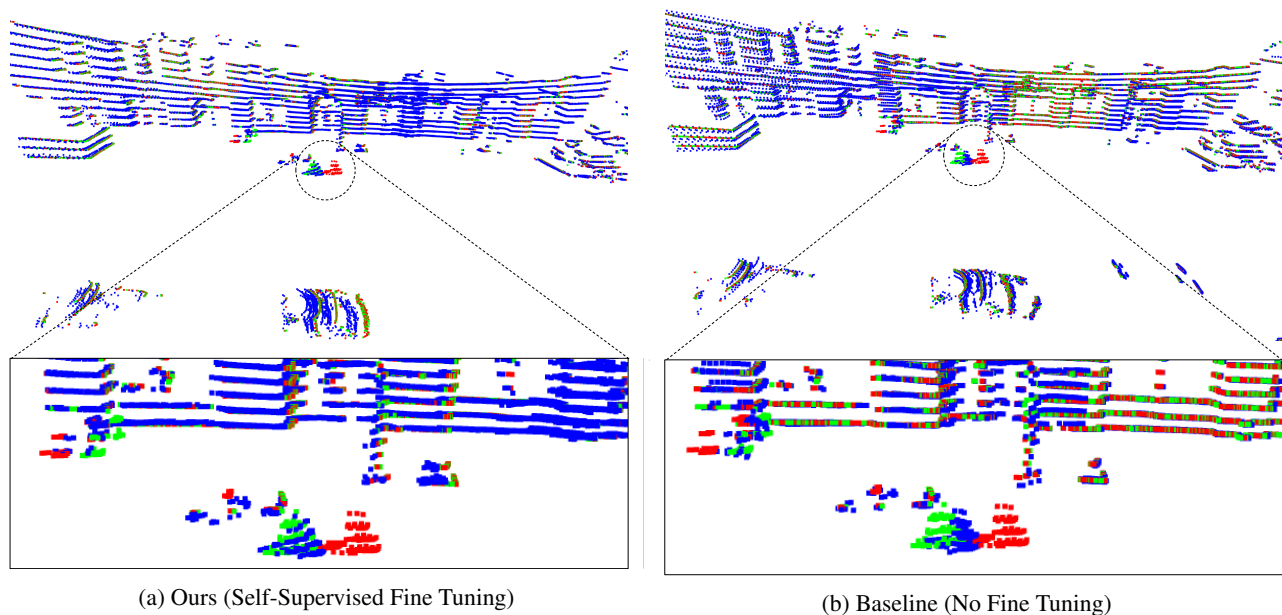


Figure 5: Comparison of our self-supervised method vs baseline on unannotated nuScenes dataset. Scene flow is computed between point cloud at time t (red) and $t + 1$ (green) and the transformed cloud is shown in blue. In our method, the predicted point cloud has a much better overlap with the point cloud of the next timestamp as compared to the baseline. Since nuScenes dataset does not provide any scene flow annotation, the supervised approaches cannot be fine tuned to this environment.

50 scenes for testing. We remove ground points from every scene analogous to the previous methods of scene flow estimation [10, 6]. Every scene consists of a pair of point clouds recorded at two different times as well as the ground

truth scene flow for every point of the first point cloud.

nuScenes The nuScenes [4] dataset is a large-scale public dataset for autonomous driving. It consists of 850 pub-

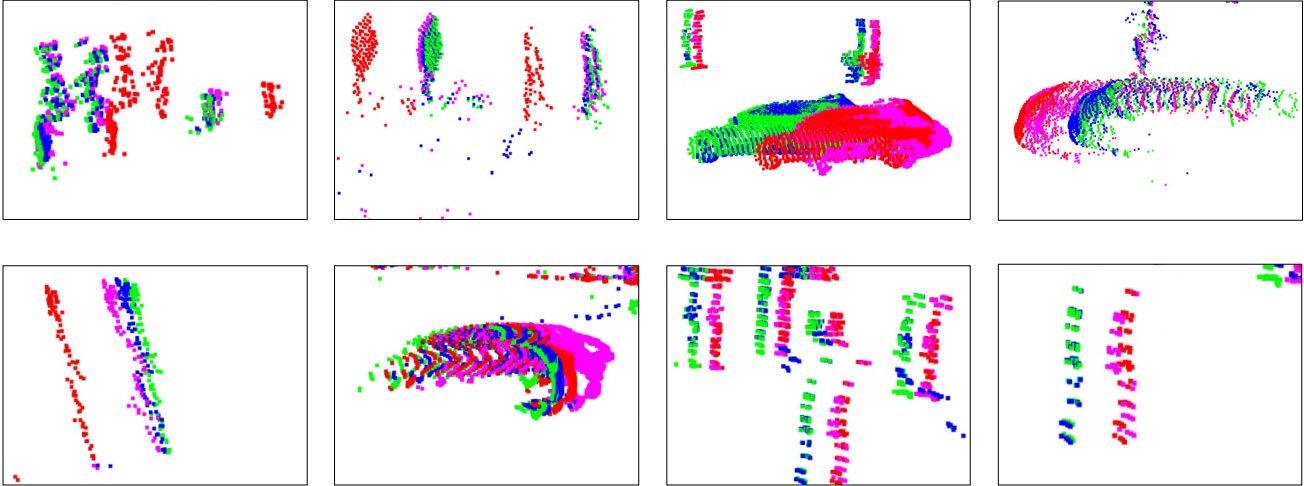


Figure 6: Improved scene flow estimation on annotated lidar data from the KITTI dataset between point cloud at time t (red) and $t + 1$ (green). Our method, which is fine tuned on nuScenes using the self-supervised loss and KITTI using a supervised loss is shown in blue. The baseline method is fine tuned only on KITTI using a supervised loss and is shown in purple. While in aggregate, both methods well estimate the scene flow, the augmented training method (blue) is able to more closely match the next frame point cloud (green). In several of the cropped scenes, the purely supervised method (purple) underestimates the flow, staying too close to the initial point cloud (red). (Best viewed in color)

licly available driving scenes in total from Boston and Singapore. The LIDAR data was collected using a Velodyne 32 LIDAR rotating at 20 Hz. This is in contrast to the 64-beam Velodyne rotating at 10 Hz used for the KITTI dataset. This difference in sensors leads to a difference in data sparsity that creates a distribution shift between KITTI and nuScenes. This distribution shift necessitates additional training on KITTI beyond our self-supervised training on nuScenes. Nonetheless, our results show a substantial benefit from the self-supervised training on nuScenes.

While the nuScenes dataset [4] contains annotations for object detection and tracking, annotations for scene flow are not available. We use this dataset for the purpose of self-supervised learning. In our experiments, out of the 850 scenes available, we use 700 as the train set and the rest 150 as the validation set. Similar to KITTI, we remove the ground points from each point cloud, using manually tuned height thresholds.

4.3. Evaluation Metric

We use three standard metrics to quantitatively evaluate the predicted scene flow when the ground truth annotations of scene flow are available. Our primary evaluation metric is End Point Error (EPE) which describes the mean Euclidean distance between the predicted and ground truth transformed points, described by the Equation 1. We also compute accuracy at two threshold levels, Acc(0.05) as the percentage of scene flow prediction with an EPE $< 0.05m$ or relative error $< 5\%$ and Acc(0.1) as percentage of points

having an EPE $< 0.1m$ or relative error $< 10\%$. These thresholds match the standard accuracy threshold computed in scene flow research.

4.3.1 Self-supervised training on nuScenes and KITTI

Unlike previous work, we are not restricted to annotated point cloud datasets. Our method can be implemented on any real-world sequential point cloud dataset. There have been several point cloud datasets published containing real lidar captures taken in urban scenes, but most of them do not contain scene flow annotations. Due to lack of annotations, these datasets can not be utilized for supervised scene flow learning. In contrast, our unsupervised loss allows us to easily integrate them into our training set. The combination of these datasets contains 5x more real data than using KITTI alone.

Setup We begin with training our self-supervised model on nuScenes dataset using the combination of Nearest Neighbor Loss and Anchored Cycle loss. Since we wish to use Flownet3D as our scene flow estimation module, we initialize our network with Flownet3D weights pretrained on FlyingThing3D dataset [11, 10]. Once the model has been trained on nuScenes, we fine-tune on KITTI in a self-supervised manner. For the comparison with the baseline, we use the Flownet3D model pretrained on FlyingThings3D without any fine-tuning on KITTI.

Training Method	EPE	ACC (0.05)	ACC (0.1)
No Fine Tuning	0.122	25.37%	57.85%
KITTI (Supervised)	<i>0.100</i>	31.42%	66.12%
Ablation: KITTI (Self-Supervised)	0.126	32.00%	73.64%
Ours: nuScenes (Self-Supervised) + KITTI (Self-Supervised)	0.1053	46.48%	79.42%
Ours: nuScenes (Self-Supervised) + KITTI (Supervised)	0.0912	47.92%	79.63%

Table 1: Comparison of levels of supervision on KITTI dataset. The nearest neighbor + anchored cycle loss is used for nuScenes (self-supervised) and KITTI (self-supervised).

Quantitative Study Using only unannotated data, we are able to achieve nearly the same performance as supervised fine tuning, in terms of endpoint error, by producing an error estimate of only 8 mm greater than those given by the supervised model. Additionally, we achieve a significantly higher accuracy with respect to both standard error thresholds. We compare our self-supervised method to the supervised fine tuning describe in [10], over various levels of supervision and self-supervision, using the same initial weights across all methods. The results of each of these methods are shown in Table 1.

Qualitative Study We compare our self-supervised method on KITTI with the baseline method in Figure 4. In this figure, both our method and the baseline have not seen the ground truth. The figure shows the point cloud captured at time t , \mathcal{X} , and $t + 1$, \mathcal{Y} , in red and green respectively. The predictions from our method are shown in blue and the baseline predictions are shown in purple. Ideally, the scene flow prediction should have a large overlap with the point cloud \mathcal{Y} . We can observe from the figure that the translated points predicted by the baseline are considerably farther from the point cloud \mathcal{Y} , in comparison to the predictions of our method, and the difference is more pronounced for scene objects exhibiting large motion. We believe this is because the baseline, trained only on synthetic FlyingThings3D, fails to completely generalize to the real-world KITTI dataset. On the contrary, our self-supervised approach can be fine tuned on any real world environment and shows a significant improvement over the baseline. The scene flow prediction from our method coincides well with the point cloud \mathcal{Y} across scene objects showing wide range of motion.

4.3.2 Self-supervised results on nuScenes

Qualitative Study We compare our method which is trained on nuScenes in a self-supervised manner with the baseline being trained on Flyingthings3d in a supervised way, by testing it over the nuScenes dataset. Figure 5 showcases the advantages of self-supervision on real world data over purely synthetic supervised training. In each

Self-Supervised Training (nuScenes + KITTI)						
NN Loss	Cycle Loss	Anchor Points	Flip	EPE (m)	ACC (0.05)	ACC (0.1)
✓	✓	✓	✓	0.1053	46.48	79.42
✓	✓	✓		0.1072	40.03	72.20
✓	✓			0.1456	30.21	48.57
✓				0.1083	42.00	78.51
				0.1258	31.99	73.63
Unsupervised (nuScenes) + Supervised Training (KITTI)						
NN Loss	Cycle Loss	Anchor Points	Flip	EPE (m)	ACC (0.05)	ACC (0.1)
✓	✓	✓	✓	0.0912	47.92	79.63
✓	✓	✓		0.0926	40.69	74.50
✓	✓			0.0916	30.76	72.94
✓				0.1144	31.24	64.58
				0.1003	31.42	66.12

Table 2: Ablation Study on the KITTI dataset. We study the effects of different self-supervised losses and data augmentation. All models are trained using the self-supervised on nuScenes and KITTI, top, and fine tuned with supervised loss, bottom.

scene, point cloud \mathcal{X} is shown in red and point cloud \mathcal{Y} is shown in green. The translated points predicted by our model and the baseline are shown in blue and purple respectively. As we can observe in the figure, the prediction from our self-supervised model has a much better overlap with point cloud \mathcal{Y} as compared to the prediction from the baseline method. The low performance of the baseline can be attributed to its training on synthetic FlyingThing3D dataset where the scale of scene flow values is considerably different than the real-world nuScenes dataset. Due to this discrepancy in the magnitude of scene flow between the datasets, the baseline is unable to generalize well to nuScenes. Moreover, since nuScenes does not have any scene flow ground truth available, the purely supervised baseline cannot be fine tuned to improve its prediction on this environment. Since our method does not rely on ground truth scene flow labels, it can be easily applied to such datasets to obtain a considerably better scene flow prediction.

4.3.3 Supervised fine tuning on KITTI

Setup In order to evaluate the performance of our method on the real-world datasets having ground truth flow annotations, we fine tune our model on KITTI. For our method, we pretrain the model on nuScenes using our self-supervised loss, and then introduce the KITTI data for supervised fine tuning. For the baseline, we use Flownet3d which is supervised fine tuned over the KITTI dataset. Both models are initialized with Flownet3D weights pretrained on FlyingThings3D.

Quantitative Results By first training on the large amount of unannotated data available in nuScenes using the combination of Nearest Neighbor Loss and Anchored Cycle Loss and then fine tuning on KITTI using the supervised loss, we are able to outperform the state-of-the-art on KITTI, obtaining an EPE of 0.0912. This is due to the fact that the additional unsupervised data allowed the model to generalize better to new real world scenes.

Qualitative Study Qualitative results can be seen in Figure 6. In each scene, point cloud \mathcal{X} is shown in red and point cloud \mathcal{Y} is shown in green. The translated points predicted by our method and the baseline are shown in blue and purple respectively. As we can observe in the figure, the prediction from our self-supervised method has a much closer overlap with point cloud \mathcal{Y} as compared to the prediction from the baseline. The baseline, however, predicts small motion, keeping the transformed cloud (purple) too close to the initial position (red). As discussed above, this bias towards small motion is due to the training of the baseline over a synthetic dataset which affects the generalization of the baseline to real-world unconstrained datasets such as KITTI where objects exhibit higher variance in motion (scene flow). By training over a significantly larger dataset, our method is able to avoid over fitting and generalize better to the scenes and flow patterns which were not present in the supervised dataset.

4.4. Ablation Studies

We test the importance of each component of our method by running a series of ablation studies. Table 2 shows the effects of iteratively removing portions of our method in both the purely self-supervised and supervised training. The advantage of implementing the anchored cycle consistency loss can be seen best in the augmented supervised results, as well as in Figure 7. We observe that by introducing the temporal flip augmentations in the train set, the model sees a wider variety of scene flow directions which reduces any directional bias present in self driving datasets. Introducing the anchor point cloud as part of the backward leg of the cycle greatly contributes towards improving the performance.

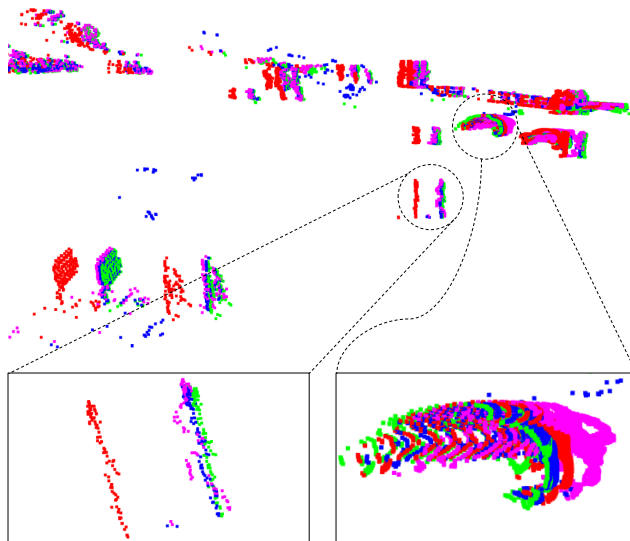


Figure 7: Ablation study comparing our self-supervised method with full self-supervised loss (blue, nearest neighbor loss + anchored cycle consistency loss) versus training only using the nearest neighbor loss (purple). Scene flow is computed between point clouds from the KITTI dataset at time t (red) and $t + 1$ (green)

This suggests that having anchored point clouds alleviates variance in the cycle consistency loss.

5. Conclusion

In this work, we propose a method for scene flow estimation in a self-supervised manner using a combination of losses: cycle-consistency loss and nearest neighbor loss. Our self supervised method is able to achieve a performance comparable to that of the supervised methods emphasizing that our approach can generalize well to the real-world datasets. We further show that once our model, trained self-supervised on a large-scale unannotated dataset, is finetuned in a supervised manner over annotated dataset, it outperforms current-state-of-the-performance. Moreover, by augmenting the datasets with the reversed point clouds, we are eliminating a bias towards one single temporal direction which is present in the dataset. Finally, we try to limit the error in our predictions by using anchored point clouds which stabilize the input used in the backward flow prediction. With our self-supervision method producing equivalent results when compared to direct supervision, it opens the door to fine tuning on arbitrary environments and future investigation into online flow learning using only sequential point clouds.

References

- [1] Tali Basha, Yael Moses, and Nahum Kiryati. Multi-view scene flow estimation: A view centered variational approach. *IJCV*, 101(1), 2013. 2
- [2] Aseem Behl, Despoina Paschalidou, Simon Donne, and Andreas Geiger. Pointflownet: Learning representations for rigid motion estimation from point clouds. In *CVPR*, 2019. 2
- [3] Paul J Besl and Neil D McKay. Method for registration of 3-d shapes. In *Sensor fusion IV: control paradigms and data structures*, volume 1611, pages 586–606. International Society for Optics and Photonics, 1992. 3
- [4] Holger Caesar, Varun Bankiti, Alex H. Lang, Sourabh Vora, Venice Erin Liong, Qiang Xu, Anush Krishnan, Yu Pan, Giancarlo Baldan, and Oscar Beijbom. nusenes: A multimodal dataset for autonomous driving. *arXiv preprint arXiv:1903.11027*, 2019. 5, 6
- [5] Andreas Geiger, Philip Lenz, and Raquel Urtasun. Are we ready for autonomous driving? the kitti vision benchmark suite. In *CVPR*, 2012. 4
- [6] Xiuye Gu, Yijie Wang, Chongruo Wu, Yong Jae Lee, and Panqu Wang. Hplflownet: Hierarchical permutohedral lattice flownet for scene flow estimation on large-scale point clouds. In *CVPR*, 2019. 1, 2, 5
- [7] Simon Hadfield and Richard Bowden. Kinecting the dots: Particle based scene flow from depth sensors. In *ICCV*, 2011. 2
- [8] Kaveh Hassani and Mike Haley. Unsupervised multi-task feature learning on point clouds. In *ICCV*, 2019. 2
- [9] Evan Herbst, Xiaofeng Ren, and Dieter Fox. Rgb-d flow: Dense 3-d motion estimation using color and depth. In *ICRA*, 2013. 1
- [10] Xingyu Liu, Charles R Qi, and Leonidas J Guibas. Flownet3d: Learning scene flow in 3d point clouds. In *CVPR*, 2019. 1, 2, 3, 4, 5, 6, 7
- [11] Nikolaus Mayer, Eddy Ilg, Philip Hausser, Philipp Fischer, Daniel Cremers, Alexey Dosovitskiy, and Thomas Brox. A large dataset to train convolutional networks for disparity, optical flow, and scene flow estimation. In *CVPR*, 2016. 3, 4, 6
- [12] Moritz Menze and Andreas Geiger. Object scene flow for autonomous vehicles. In *CVPR*, 2015. 2
- [13] Moritz Menze, Christian Heipke, and Andreas Geiger. Joint 3d estimation of vehicles and scene flow. *ISPRS Annals of Photogrammetry, Remote Sensing & Spatial Information Sciences*, 2, 2015. 3
- [14] Moritz Menze, Christian Heipke, and Andreas Geiger. Object scene flow. *ISPRS Journal of Photogrammetry and Remote Sensing*, 140, 2018. 3
- [15] Ishan Misra, C Lawrence Zitnick, and Martial Hebert. Shuffle and learn: unsupervised learning using temporal order verification. In *ECCV*, 2016. 2
- [16] Charles R Qi, Hao Su, Kaichun Mo, and Leonidas J Guibas. Pointnet: Deep learning on point sets for 3d classification and segmentation. In *Proceedings of the IEEE Conference on Computer Vision and Pattern Recognition*, pages 652–660, 2017. 2
- [17] Charles Ruizhongtai Qi, Li Yi, Hao Su, and Leonidas J Guibas. Pointnet++: Deep hierarchical feature learning on point sets in a metric space. In *Advances in neural information processing systems*, pages 5099–5108, 2017. 2
- [18] Levi Valgaerts, Andrés Bruhn, Henning Zimmer, Joachim Weickert, Carsten Stoll, and Christian Theobalt. Joint estimation of motion, structure and geometry from stereo sequences. In *ECCV*, 2010. 2
- [19] Victor Vaquero, Alberto Sanfeliu, and Francesc Moreno-Noguer. Deep lidar cnn to understand the dynamics of moving vehicles. In *ICRA*, 2018. 2
- [20] Sundar Vedula, Simon Baker, Peter Rander, Robert Collins, and Takeo Kanade. Three-dimensional scene flow. In *ICCV*, 1999. 2
- [21] Christoph Vogel, Konrad Schindler, and Stefan Roth. 3d scene flow estimation with a rigid motion prior. In *ICCV*, 2011. 2
- [22] Christoph Vogel, Konrad Schindler, and Stefan Roth. Piecewise rigid scene flow. In *ICCV*, 2013. 2
- [23] Christoph Vogel, Konrad Schindler, and Stefan Roth. 3d scene flow estimation with a piecewise rigid scene model. *IJCV*, 115(1), 2015. 2
- [24] Shenlong Wang, Simon Suo, Wei-Chiu Ma, Andrei Pokrovsky, and Raquel Urtasun. Deep parametric continuous convolutional neural networks. In *CVPR*, 2018. 1, 2
- [25] Xiaolong Wang and Abhinav Gupta. Unsupervised learning of visual representations using videos. In *ICCV*, 2015. 2
- [26] Xiaolong Wang, Allan Jabri, and Alexei A Efros. Learning correspondence from the cycle-consistency of time. In *CVPR*, 2019. 2